Hindawi
International Journal of Antennas and Propagation
Volume 2023, Article ID 7718693, 14 pages
https://doi.org/10.1155/2023/7718693

Research Article

Side Null Analysis of the Main-Auxiliary Antenna Array for Noncooperative Interference Cancellation

ZheYu Li, JiaHao Zhang, YaXing Li, FangMin He, HongZhang Gao, and Jin Meng

National Key Laboratory of Science and Technology on Electromagnetic Energy, Naval University of Engineering, Wuhan 430000, China

Correspondence should be addressed to JiaHao Zhang; jiahao.z@hotmail.com

Received 14 August 2023; Revised 29 October 2023; Accepted 20 November 2023; Published 30 November 2023

Academic Editor: Giuseppe Torrisi

In interference cancellation, the null at the angle of arrival (AoA) of interference can suppress interference. However, due to the large spacing between array elements and the periodicity of the array, some small nulls at the angles of noninterference are formed inevitably. When the AoA of the desired signal is in these small nulls, they impair the effectiveness of interference cancellation by attenuating the desired signal. This paper proposes the concept of a side null to represent these nulls in the noninterference direction. And the cancellation ratio of the desired signal (SCR) is deduced to quantitatively characterize the side null. The spatial noncooperative interference cancellation model based on the main-auxiliary antenna array is established. Based on this, the SCR is derived to evaluate the amount of desired signal attenuation. Then the simulation, respectively, in two-dimensional plane and three-dimensional space, describes the side null visually. Moreover, the method of side null reduction is discussed by modulation of the array. Finally, the existence of side null and its influence on interference cancellation are verified through the experiments. The results of the simulation and experiment are in good agreement, and both support the theoretical analysis.

1. Introduction

To solve electromagnetic interference, interference cancellation is an important electromagnetic compatibility technology in both civil and military applications [1, 2]. The interference cancellation system synthesizes cancellation signal by sampling the interference signal. Then, the cancellation signal is cancelled with the interference signal from the desired signal in equal amplitude and inverse phase [3]. It is shown in the spatial domain that the null is formed at the angle of arrival (AoA) of the interference signal to suppress it [4]. Interference can be divided into self-interference and noncooperative interference. The self-interference generally comes from the cooperative platform, and the signal is known. Interference cancellation can take advantage of the prior knowledge of the interference signal [5–7]. However, as for noncooperative interference, the interference signal is completely unknown. They can be intentional adversarial interference or unintentional high-power interference [8, 9]. Therefore, interference sampling becomes much more difficult than self-interference. To solve the challenge of sampling interference, it is common to load auxiliary antennas, forming the antenna array [10–12]. However, how to arrange these auxiliary antennas, that is, the manifold of the array and the radiation pattern it forms, is decisive to the effectiveness of interference cancellation. This paper is to analyze, in noncooperative interference cancellation, one kind of null feature of the radiation pattern formed by an array with inconsistent main and auxiliary antennas and its effect on interference cancellation.

From the perspective of the spatial domain, interference cancellation can be issued because the radiation pattern of the array forms the null at AoA of the interference signal. It reduces the array gain on the interference signal to suppress interference [13, 14]. However, in the simulation and measurement, some small nulls in the angles of non-interference can be observed obviously. These small nulls are undesired. When AoA of the desired signal is in these small nulls, the effectiveness of interference cancellation is impaired unequally. In order to research the effect of these nulls

on interference cancellation, the null at AoA of the interference is described as the main null, and those small nulls at AoA of noninterference are described as the side nulls, respectively, with reference to the definitions of main lobe and side lobe.

The main null and side null are important features for interference cancellation, just as main lobe and side lobe are important for beamforming. The main lobe is the main direction of radiation, while the side lobe generally appears around the main lobe because of the large spacing between array elements and the periodicity of the array, which would disperse the power of the main lobe [15]. Thus, many papers have discussed the side lobe and proposed various methods to suppress it [16–18]. They mainly include optimizing the array by the optimization algorithm [19, 20], improving the antenna structure [21, 22], and superposing the radiation pattern to suppress the side lobe [23, 24]. The studies in [25] combines the metasurface with amplitude and phase controllable unit cell, and realize the side-lobe levels suppression of a metasurface lens. Reference [26] proposes a 2D joint iterative adaptive filtering method by adopting the reiterative minimum mean square error (RMMSE) criterion to reduce the side lobe. Some papers consider both the side-lobe reduction and anti-interference performance of the array. The studies in [27] introduces the bat algorithm (BA) to the uniformly spaced linear array (ULA). It suppresses the side lobe and also discusses the null formed at the interference directions. The studies in [28] proposes an adaptive null broadening method for suppression of rapidly moving interferences. However, most papers only concern themselves with the null generated in interference directions and pay no attention to the null in noninterference directions that may attenuate the desired signal. Reference [29] considers the desired signal loss incurred by interference nulling, but it is for the situation when the arrival direction of the interference signal and the desired signal are similar. In [30], the grating null is mentioned to affect spatial interference reduction in GPS receivers, but it is not clearly characterized in the paper. Table 1 compares the research in different applications between parts of similar references and this paper. For the common omnidirectional main antenna, the side nulls are obvious and have a significant effect on the desired signal. Therefore, it is necessary to characterize the side null quantitatively and analyze its influencing factors.

It is known that the purpose of interference cancellation is to eliminate interference signals and reserve desired signals. In the spatial domain, the main null is formed in the AoA of the interference signal to reduce interference. However, due to the existence of the side null, when the AoA of the desired signal is on the side null, the desired signal is also suppressed. In this way, even if the interference is cancelled, the desired signal is also attenuated. Therefore, the communication based on the desired signal is unable to recover to the level before interference. The effectiveness of interference cancellation decreases, that is, the interference cancellation is affected by the side null. In fact, the effect of side null with different depths on interference cancellation is different, so the quantitative characterization is essential for estimating its influence. Considering that the side null affects interference cancellation by affecting the reception of the desired signal, the amount of the desired signal attenuation is used to characterized the side null. The attenuation of the desired signal is also described as the cancellation ratio of the desired signal (SCR).

This paper focuses on the side null of the main-auxiliary antenna array in noncooperative interference cancellation. The concept of the side null is proposed through practical phenomena. Then, the concept is characterized quantitatively through modeling and derivation. Finally, it is verified by simulation and experiment. The major works of this paper are summarized as follows:

(1) Compared with most papers that mainly discuss the characteristics of the lobe or the null at AoA of interference in radiation pattern, this paper focuses on the null at noninterference directions in interference cancellation and proposes the concept of the side null through the practical phenomenon of interference cancellation.

(2) The side null is characterized quantitatively by the attenuation of the desired signal and is verified by simulation and experiment.

(3) The methods of reducing side null by modifying arrays are discussed, which provides possibilities for the subsequent research of side null suppression.

The paper is organized as follows. Section 2 establishes the noncooperative interference cancellation spatial model based on the main-auxiliary antenna array. Section 3 deduces the SCR to characterize the side null quantitatively and analyzes the influence factors of input signal power and antenna pattern. The simulation in two-dimensional plane and three-dimensional space is also discussed. Section 4 discusses three methods to realize side null reduction through adjusting the array. The experiment is conducted in Section 5 to verify the existence of the side null and its influence on interference cancellation. Finally, conclusions are drawn in Section 6.

2. System Model for Noncooperative Interference Cancellation

2.1. Model of the Main-Auxiliary Antenna Array. The schematic diagram of spatial noncooperative interference cancellation is shown in Figure 1. The interference signal is from the noncooperative platform, and its power is much higher than the desired signal. The AoA of the interference signal and the desired signal are different. Figure 2 shows the established coordinate system. $\theta \in [0, \pi]$ is the pitch angle and $\varphi \in [-\pi, \pi]$ is the azimuth angle in the coordinate system. $G(\theta, \varphi)$ represents the radiation pattern of main antenna. The column vector $\mathbf{g}(\theta, \varphi) = [g_1(\theta, \varphi), g_2(\theta, \varphi), \cdots g_M(\theta, \varphi)]^T$ represents M radiation patterns of auxiliary antennas. Because the main antenna undertakes the function of transmitting and receiving high-power communication signals, it tends to be larger in gain and size than the auxiliary antenna, which constitutes the main-auxiliary antenna array. The position of the main antenna is located at the

Table 1: Comparision of similar references.

References	Application	The feature of radiation pattern	The methods adopted
[31]	Array pattern synthesis	Main lobe and side lobe	Maximize main lobe using convex optimization with side-lobe constraints
[32]	Interference suppression	The null at interference direction	Propose a dual ring antenna to form null at interference direction
[27]	Interference suppression	The null at interference direction	Use adaptive bat algorithm (BA) to impose nulls at directions of interferences
[33]	Multiple interferences suppression	The null at interference direction in main-lobe and/or side-lobe	Form the coupling nulls of space and polarization domain
[28]	Rapidly moving interference suppression	The null at interference direction	Broaden the null at interference direction
[30]	Spatial interference reduction	Grating nulls at noninterference directions	Describe grating null mainly by simulation
This paper	Interference cancellation	Side null at noninterference directions	Quantitatively characterize the effect of side null on interference cancellation

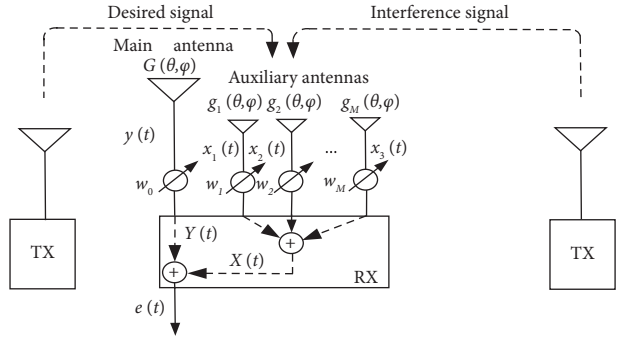

Figure 1: Schematic diagram of noncooperative interference cancellation.

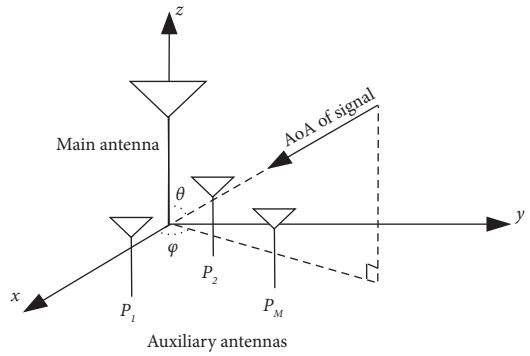

Figure 2: The coordinate system of the main-auxiliary antenna array.

coordinate origin. $\mathbf{P} = [\mathbf{P}_1, \mathbf{P}_2, \cdots \mathbf{P}_M]^T$ represents the position coordinates of auxiliary antennas, and the coordinate of the M^{th} auxiliary antenna is $\mathbf{P}_M = [x_m, y_m, z_m]$. The phase of arrival signal for the main antenna is regarded as the standard phase, then the signal phase differences for auxiliary antennas are $\phi(\theta, \varphi) = [\phi_1, \phi_2, \cdots \phi_M]^T$, where

$$\phi_M(\theta, \varphi, x, y, z) = \frac{2\pi}{\lambda}(x \sin\theta \cos\varphi + y \sin\theta \sin\varphi + z \cos\theta). \tag{1}$$

Thus, the array manifold of the auxiliary antennas can be expressed as follows:

$$\mathbf{A}_{\mathbf{a}}(\theta, \varphi) = [\mathbf{g}(\theta, \varphi) \odot \exp[j\boldsymbol{\phi}(\theta, \varphi, x, y, z)]]^T. \tag{2}$$

It is assumed that the AoA of interference signal $i(t)$ is (θ_i, φ_i), and the power is P_i. The AoA of the desired signal $s(t)$ is (θ_s, φ_s), and the power is P_s. w_0 is the weight of signal output by the main antenna, and $\mathbf{W} = [w_1, w_2, \cdots w_M]^T$ is the weights of signals output by the auxiliary antennas. Then the signal received by the main antenna is

$$y(t) = s(t)G(\theta_s, \varphi_s) + i(t)G(\theta_i, \varphi_i) + n(t), \tag{3}$$

where $n(t)$ is the received noise signal. Then the signal received by auxiliary antennas is

$$\mathbf{x}(t) = s(t)\mathbf{A}_{\mathbf{a}}(\theta_s, \varphi_s) + i(t)\mathbf{A}_{\mathbf{a}}(\theta_i, \varphi_i) + \mathbf{n}(t). \tag{4}$$

Therefore, the output signal after the interference cancellation is

$$e(t) = Y(t) + X(t) = w_0 y(t) - \mathbf{W}^H \mathbf{x}(t). \tag{5}$$

And the synthetic radiation pattern of the antenna array is

$$G_s(\theta, \varphi) = w_0 G(\theta, \varphi) - \mathbf{W}^H \mathbf{A}_{\mathbf{a}}(\theta, \varphi). \tag{6}$$

2.2. Power Inversion Criterion. In interference cancellation, the optimal weights are obtained based on the output criterion. Power inversion (PI) is a commonly used cancellation algorithmic criterion, which is suitable for the case of strong interference and the weak desired signal. It regards the output signal as the error signal, and the weights are calculated to minimize the power of the error signal. Its performance function can be expressed as follows:

$$\xi = E\left[|e(t)|^2\right]. \tag{7}$$

It can be converted into a minimum problem of $\min \xi = E[|e(t)|^2]$. To avoid the occurrence of invalid solution of 0, $w_0 = 1$ is set as the constraint. Equation (5) is substituted into (7) and we get

$$\begin{aligned}\xi &= E\left[|e(t)|^2\right] = E\left[e(t)e^*(t)\right] \\ &= E\left[|y(t)|^2\right] - 2\mathrm{Re}\left[\mathbf{W}^H\mathbf{r}_{\mathbf{xy}}\right] + \mathbf{W}^H\mathbf{R}_{\mathbf{xx}}\mathbf{W},\end{aligned} \tag{8}$$

where $\mathbf{R_{xx}}$ is the autocorrelation matrix of $\mathbf{x}(t)$ and $\mathbf{r_{xy}}$ is the cross-correlation matrix of $\mathbf{x}(t)$ and $y(t)$. The optimal solution of weight can be obtained as follows:

$$\mathbf{W}_{\mathrm{opt}} = \mathbf{R}_{xx}^{-1}\mathbf{r}_{xy}. \tag{9}$$

When the desired signal, interference signal, and noise signal are mutually incoherent, $\mathbf{R}_{xx}$ can be expressed as follows:

$$\mathbf{R}_{xx} = \mathbf{R}_{ss} + \mathbf{R}_{ii} + \mathbf{R}_{nn}, \tag{10}$$

where, $\mathbf{R}_{ss}$, $\mathbf{R}_{ii}$, and $\mathbf{R}_{nn}$ is the autocorrelation matrix of the desired signal $s(t)$, interference signal $i(t)$, and noise signal $n(t)$, respectively. Because the power of interference signal is much higher than the desired signal, $\mathbf{R}_{ss}$ can be ignored. $\mathbf{R}_{xx}$ can be written approximately as follows:

$$\begin{aligned}\mathbf{R}_{xx} &\approx \mathbf{R}_{ii} + \mathbf{R}_{nn} \\ &= p_i\mathbf{A}_{\mathbf{a}}(\theta_i,\varphi_i)\mathbf{A}_{\mathbf{a}}^H(\theta_i,\varphi_i) + \sigma^2\mathbf{I} \\ &= \sigma^2\mathbf{I} + \mathbf{A}_{\mathbf{a}}(\theta_i,\varphi_i)\cdot p_i\mathbf{I}\cdot\mathbf{A}_{\mathbf{a}}^H(\theta_i,\varphi_i),\end{aligned} \tag{11}$$

where σ^2 is the noise power and $\mathbf{I}$ is the identity matrix. According to the matrix inversion lemma:

$$(\mathbf{A}+\mathbf{BCD})^{-1} = \mathbf{A}^{-1} - \mathbf{A}^{-1}\mathbf{B}\left(\mathbf{C}^{-1} + \mathbf{D}\mathbf{A}^{-1}\mathbf{B}\right)^{-1}\mathbf{D}\mathbf{A}^{-1}. \tag{12}$$

$\mathbf{R}_{xx}$ is inverted and is written as

$$\begin{aligned}\mathbf{R}_{xx}{}^{-1} &= \frac{1}{\sigma^2}\mathbf{I} - \frac{1}{\sigma^2}\mathbf{I}\cdot\mathbf{A}_{\mathbf{a}}(\theta_i,\varphi_i) \\ &\quad\cdot\left(\frac{1}{p_i}\mathbf{I} + \mathbf{A}_{\mathbf{a}}^H(\theta_i,\varphi_i)\cdot\frac{1}{\sigma^2}\mathbf{I}\cdot\mathbf{A}_{\mathbf{a}}(\theta_i,\varphi_i)\right)^{-1}\cdot\mathbf{A}_{\mathbf{a}}^H(\theta_i,\varphi_i)\cdot\frac{1}{\sigma^2} \\ &= \frac{1}{\sigma^2}\cdot\left(\mathbf{I} - \frac{p_i\mathbf{A}_{\mathbf{a}}(\theta_i,\varphi_i)\mathbf{A}_{\mathbf{a}}^H(\theta_i,\varphi_i)}{\sigma^2 + Mp_i}\right).\end{aligned} \tag{13}$$

And the cross-correlation matrix $\mathbf{r}_{xy}$ can be written as

$$\mathbf{r}_{xy} \approx p_iG(\theta_i,\varphi_i)\mathbf{A}_{\mathbf{a}}(\theta_i,\varphi_i) + \sigma^2\mathbf{I}_{M\times 1}. \tag{14}$$

Therefore, the optimal weight can be expressed as

$$\begin{aligned}\mathbf{W}_{\mathrm{opt}} &= \mathbf{R}_{xx}^{-1}\mathbf{r}_{xy} \\ &= \frac{1}{\sigma^2}\cdot\left(\mathbf{I} - \frac{p_i\mathbf{A}_{\mathbf{a}}(\theta_i,\varphi_i)\mathbf{A}_{\mathbf{a}}{}^H(\theta_i,\varphi_i)}{\sigma^2 + Mp_i}\right)\cdot\left(p_iG(\theta_i,\varphi_i)\mathbf{A}_{\mathbf{a}}(\theta_i,\varphi_i) + \sigma^2\mathbf{I}_{M\times 1}\right).\end{aligned} \tag{15}$$

3. Description of Side Null

3.1. Side Null Characterization. The purpose of interference cancellation is to preserve the desired signal and to cancel the interference signal. Side null causes the attenuation of the desired signal, and thus the amount of desired signal attenuation is considered to quantitatively characterize side null. The attenuation of the desired signal is represented by the cancellation ratio of the desired signal (SCR). When SCR is less than a certain value, the null in the noninterference direction is regarded as the side null. The SCR can be expressed by the ratio between input and output signal noise ratio (SNR). The input SNR, $\mathrm{SNR_{in}}$ can be represented directly:

$$\mathrm{SNR_{in}} = \frac{P_s}{\sigma_1^2}. \tag{16}$$

And the output SNR, $\mathrm{SNR_{out}}$ can be obtained from the above modeling:

$$\mathrm{SNR_{out}} = \frac{E\left(\left|s(t)G(\theta_s,\varphi_s) - \mathbf{W}_{\mathrm{opt}}^H\mathbf{A}_{\mathbf{a}}(\theta_s,\varphi_s)\mathrm{s}(t)\right|^2\right)}{\sigma_2^2}. \tag{17}$$

Thus, substituting equations (15)–(17), SCR can be expressed as

$$
\begin{aligned}
\mathrm{SCR} &= \frac{\mathrm{SNR}_{\mathrm{out}}}{\mathrm{SNR}_{\mathrm{in}}} \\
&= \frac{E\left(\left|s(t)G(\theta_s,\varphi_s) - \mathbf{W}_{\mathrm{opt}}^H \mathbf{A}_{\mathbf{a}}(\theta_s,\varphi_s)\mathrm{s}(t)\right|^2\right)}{\sigma_2^2} \cdot \frac{\sigma_1^2}{P_s} \\
&= \frac{E\left(|s(t)|^2\right)\left[G(\theta_s,\varphi_s) - \mathbf{W}_{\mathrm{opt}}^H \mathbf{A}_{\mathbf{a}}(\theta_s,\varphi_s)\right]^2}{G^2(\theta_s,\varphi_s)\cdot\sigma_1^2} \cdot \frac{\sigma_1^2}{P_s} \\
&= \frac{\left[G(\theta_s,\varphi_s) - \mathbf{W}_{\mathrm{opt}}^H \mathbf{A}_{\mathbf{a}}(\theta_s,\varphi_s)\right]^2}{G^2(\theta_s,\varphi_s)} \\
&= \frac{1}{G^2(\theta_s,\varphi_s)} \left| G(\theta_s,\varphi_s) - \left(\frac{1}{\sigma^2} \cdot \left(\mathbf{I} - \frac{p_i \mathbf{A}_{\mathbf{a}}(\theta_i,\varphi_i)\mathbf{A}_{\mathbf{a}}^H(\theta_i,\varphi_i)}{\sigma^2 + M p_i} \right) \right)^H \mathbf{A}_{\mathbf{a}}(\theta_i,\varphi_i) \cdot \left(p_i G(\theta_i,\varphi_i)\mathbf{A}_{\mathbf{a}}(\theta_i,\varphi_i) + \sigma^2 \mathbf{I}_{M\times 1}\right) \right|^2,
\end{aligned}
\tag{18}
$$

where $\sigma_1{}^2$ and $\sigma_2{}^2$ are the input and output power of noise signals, respectively.

In further analysis, when the AoA of interference signal (θ_i, φ_i) is known, the AoA of desired signal (θ_s, φ_s) can be written as $(\theta_i + \Delta\theta, \varphi_i + \Delta\varphi)$. Where $\Delta\theta$ and $\Delta\varphi$ are the angular differences between the interference signal and desired signal in the pitch plane and azimuth plane, respectively. Therefore, in the radiation pattern after interference cancellation, the range of side null can be expressed as

$$
\begin{cases}
f(\theta,\varphi) = \mathrm{SCR} < \chi_1, & \theta \in \Theta_{SN}, \varphi \in \Theta_{SN}, \\
g(\theta,\varphi) = \sum f^{-1}(\mathrm{SCR}, \Delta\theta, \Delta\varphi), & \Delta\theta \in [0,\pi] \Delta\varphi \in [-\pi,\pi],
\end{cases}
\tag{19}
$$

where $g(\theta, \varphi)$ represents the sum of side nulls in the range.

3.2. Analysis of Influence Factors. The influence of signal input power and the pattern of main and auxiliary antennas on the side null is analyzed. For the PI algorithm, it is suitable for high input interference to signal power ratio (ISR). Thus, the signal input power is discussed in the cases of strong interference and weak desired signals. From (18), it can be seen that the SCR is related to the pattern of the main antenna $G(\theta, \varphi)$, the auxiliary array manifold $\mathbf{A}_{\mathbf{a}}(\theta, \varphi)$, and the power of interference signal P_i. The pattern of auxiliary antennas is included in $\mathbf{A}_{\mathbf{a}}(\theta, \varphi)$. For the power of the desired signal, because SCR represents the relative attenuation value of the desired signal, SCR is independent of the power of the desired signal in (18). However, under the same attenuation, different powers of the desired signal input will generate different desired signal outputs. The higher power of the desired signal output will be conducive to the subsequent desired signal inspection and amplification. For antenna pattern, because the omnidirectional antenna has no specific main lobe, the effect of the side null is more obvious. Meanwhile, the omnidirectional antenna is a representative main antenna and an auxiliary antenna, which is used for moving communication systems or systems with a nonfixed direction of desired signals. Therefore, the omnidirectional main and auxiliary antennas of different gains are analyzed subsequently. Figure 3 shows the radiation pattern of the main antenna and auxiliary antenna. Figure 4 shows the array of synthetic radiation patterns under different input interference signal powers in the two-dimensional plane of $\theta = 90^\circ$. It can be observed that higher input interference power will result in a deeper main null.

3.3. Side Null Simulation in a Two-Dimensional Plane. Taking the linear array as an example, one main antenna and three auxiliary antennas are simulated and analyzed. Three auxiliary antennas are periodically located with a uniform spacing of x, equal-height with the main antenna, as shown in Figure 5. The spacing x is taken as λ. λ is the wavelength corresponding to the signal center frequency. Input SNR and INR are set at 20 dB and 50 dB, respectively. The AoA of the interference signal is randomly selected as $(90^\circ, 45^\circ)$. To simplify the analysis, the side null is first discussed in the two-dimensional plane.

It is assumed that the AoA of the desired signal in the pitch plane is $\theta = 90^\circ$. The same as that of the interference signal. And the AoA of the desired signal in the azimuth plane, φ_s is traversed from $-\pi$ to π, and the possibility of any azimuth angle is equal. The curve of SCR changing with the AoA of desired signal φ_s is shown in Figure 6(a). It can be observed that when $\varphi_s = \varphi_i = 45^\circ$, $\mathrm{SCR}_{\mathrm{min}} = -72\mathrm{dB}$. It means that the deepest null is formed at the AoA of the interference signal $\varphi_i = 45^\circ$, which is in the main null. And

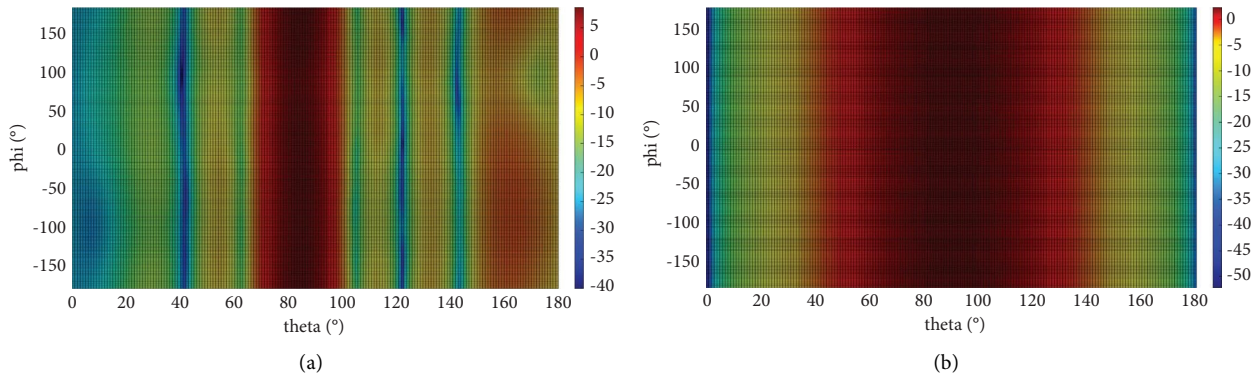

Figure 3: The radiation pattern of main antenna and auxiliary antenna. (a) The main antenna. (b) The auxiliary antenna.

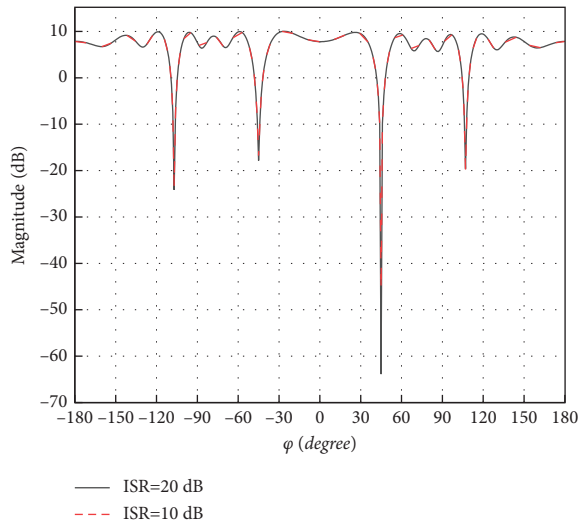

Figure 4: The array synthetic radiation pattern under different input interference signal power.

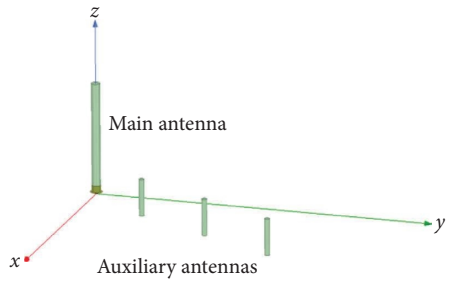

Figure 5: The simulated linear array of one main antenna and three auxiliary antennas.

when the AoA of the desired signal and the interference signal are same, the attenuation of the desired signal is maximum. As shown in Figure 6(a), the red dotted line corresponds to the AoA of the desired signal when SCR = −3dB. This means that the power of the desired signal is attenuated by half. It is assumed that the communication system is unable to communicate at this level with the desired signal. Thus, when SCR < −3dB at the AoA of the desired signal, they are described as side nulls. It is observed that when SCR < −3dB, the range of side nulls is $\varphi_s \in (-166, -160) \cup (-20, -14) \cup (131, 139)$.

Then, the side null is further analyzed in the pitch plane. When the desired signal is from the same azimuth plane $\varphi = 45^\circ$ with the interference signal, the AoA of the desired signal in the pitch plane θ_s is traversed from 0 to π and the possibility of any pitch angle is equal. The curve of SCR changing with the AoA of the desired signal θ_s is shown in Figure 6(b). It also can be seen that when $\theta_s = \theta_i = 90^\circ$,

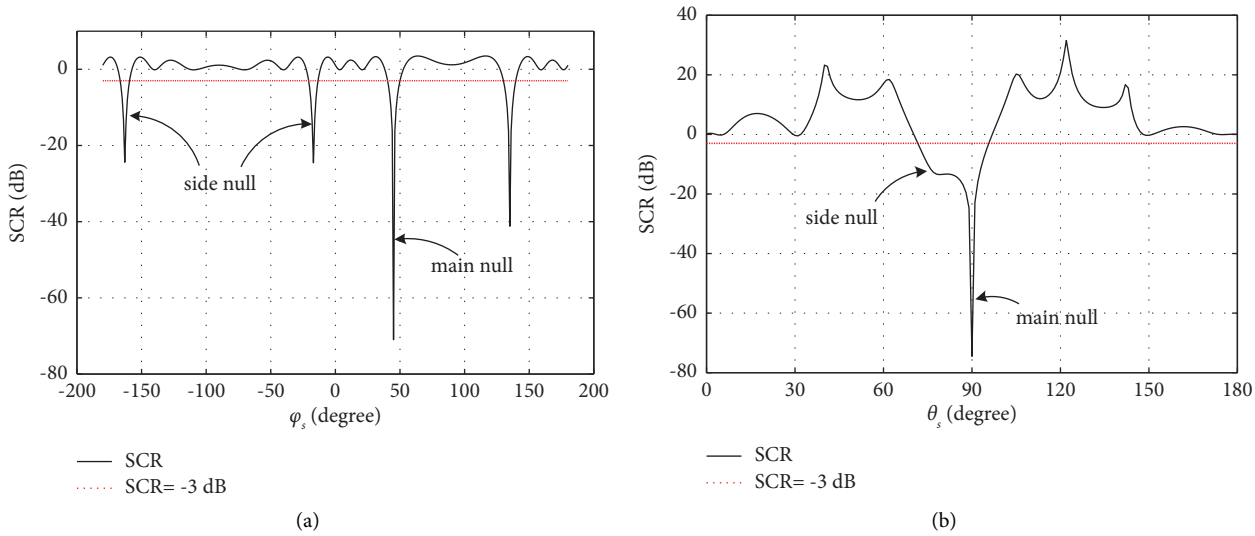

Figure 6: The side null in two-dimensional plane. (a) In the azimuth plane of $\theta = 90^\circ$. (b) In the pitch plane of $\varphi = 45^\circ$.

$\text{SCR}_{\text{min}} = -71.9\text{dB}$. The deepest null appears in the AoA of the desired signal and interference signal are same. The red dotted line corresponds to the AoA of desired signal when SCR = −3dB. It is observed that the main null and the side nulls are fused together. When SCR < −3dB, $\theta_s \in (72, 95)$.

3.4. Side Null Simulation in Three-Dimensional Space. Based on the analysis above, the side null is then discussed in three-dimensional space. The simulation conditions remain the same. However, the AoA of the desired signal is from any direction in the space. The pitch angle of desired signal θ_s is traversed from 0 to π and the azimuth angle φ_s is traversed from $-\pi$ to π. The possibility of the desired signal from any angle is equal. The curve of SCR changing with the AoA of the desired signal (θ_s, φ_s) is shown in Figure 7(a). Similarly, 3 dB is taken for the communication threshold, that is, $\chi_1 = -3$. Figure 7(b) shows the range of SCR < −3dB. It means that when the AoA of the desired signal is from these ranges, the desired signal will be attenuated more than 3 dB and the communication will be affected. Besides the main null, where the AoA of the desired signal and interference signal are the same, the side nulls in the radiation pattern after interference cancellation can be clearly observed.

4. Side Null Reduction

The side null is caused by the large array spacing and phase periodicity. Therefore, the reduction of the side null can be considered by adjusting the array manifold. In this section, the array manifold is optimized from three aspects of the array, including element spacing, element number, and array configuration, to discuss the methods of side null reduction.

4.1. The Spacing between Array Element. From the equations of (1) and (18), it can be found that SCR is affected by the spacing x. Figure 8(a) shows the proportion of side nulls in three-dimensional space when spacing x changes equidistantly from 0 to 5λ, and the other conditions keep the same. It can be observed that when the spacing x is near $\lambda/2$, the proportion of side nulls is the minimum. When $0 < x < \lambda/2$, the proportion decreases with the increasing spacing. When $x > \lambda/2$, with the increase of spacing, the proportion first increased and then decreased in the local scope, showing a certain periodicity, but it increased overall. This is related to the periodicity of the phase. But it is not completely periodic, probably due to the different gains of the main and auxiliary antennas. $x = \lambda/2$ and $x = \lambda/4$ are selected for signal simulation to verify Figure 8(a). Figure 8(b) shows the side nulls of the two spacing x. The dark blue range is the common side nulls of $x = \lambda/2$ and $x = \lambda/4$, and the light red range is the side nulls where $x = \lambda/4$ is more than $x = \lambda/2$. The proportion of side nulls is 1.41% when $x = \lambda/2$ and 3.13% when $x = \lambda/4$, respectively. It is consistent with two points of 1.44% and 3.21% in Figure 8(a).

The genetic algorithm (GA) is also used to optimize the array spacing x. The parameters of GA are set as follows. The population size is 100. The probability of crossover is 0.6, and the probability of variation is 0.01. The position of the array element is encoded in binary. Figure 8(c) shows the convergence curves with randomly selected spacing x for the initial values. The optimization results also show that when $x = \lambda/2$, the proportion of side nulls is at its minimum, about 1.38%. This is consistent with the result above.

4.2. The Number of Array Element. The array manifold $\mathbf{A_a}(\theta, \varphi)$ and SCR are both affected by the number of array element M. When other conditions remain unchanged, changing the number of array elements M will observe a change of the side null. Figure 9 shows the position and range of the side nulls under different number of auxiliary antennas. The color ranges from light to dark, showing more side nulls in small antennas number array than in the large antenna number array in sequence. It can be found that the

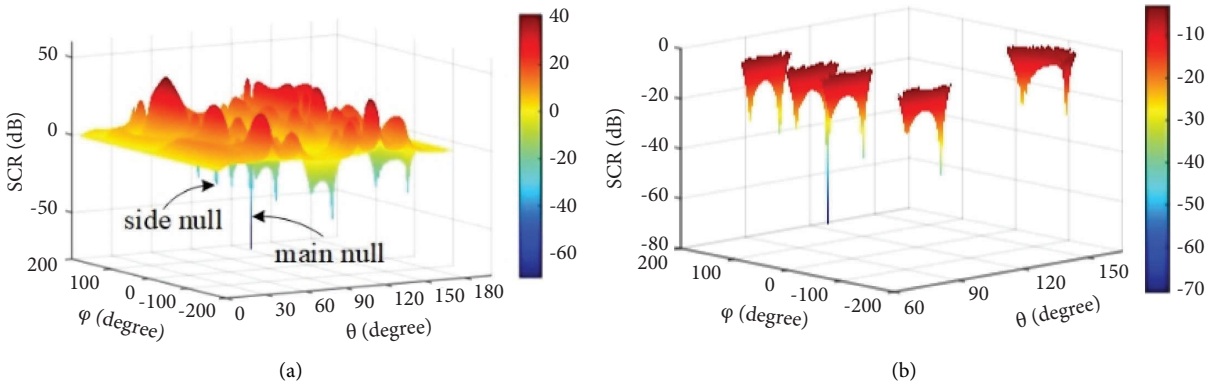

FIGURE 7: (a) The SCR in three-dimensional space. (b) The side null in three-dimensional space.

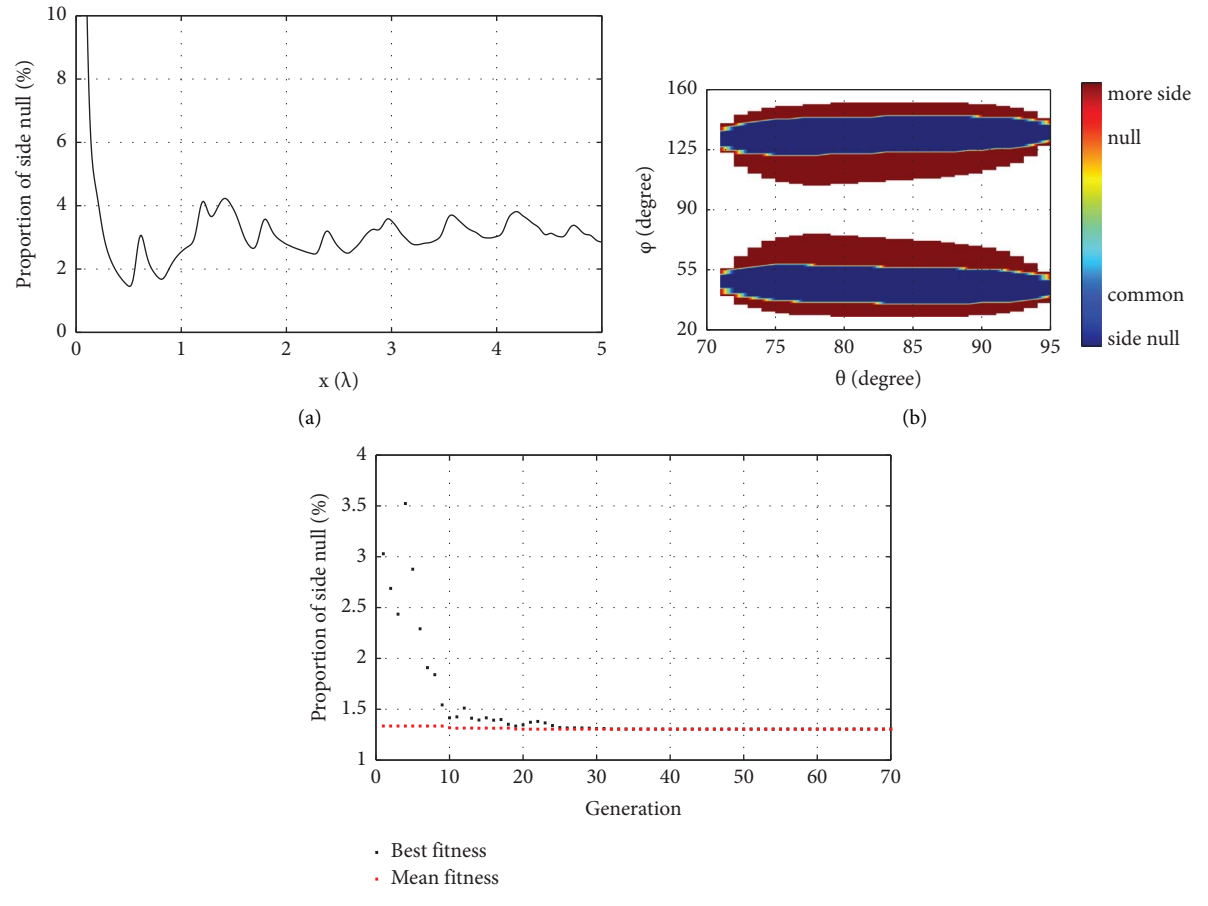

FIGURE 8: (a) The proportion of side nulls with changing spacing x. (b) The side nulls of $x = \lambda/4$ and $x = \lambda/2$. (c) The convergence curves of GA.

range of side nulls decreases when the number of auxiliary antennas increases. However, the positions of the side nulls do not change with the increase in antenna number. Table 2 shows the proportion of side nulls with different numbers of auxiliary antennas. Increasing the number of antennas can realize the reduction of the side null, but it increases the array aperture and requires more complex practical implementation.

4.3. The Configuration of the Array. The configuration of the antenna array affects SCR by affecting the array manifold $\mathbf{A}_a(\theta, \varphi)$. Taking typical one-dimensional linear array, and two-dimensional circular array, as examples, the influence of configuration on side null is analyzed. The simulated conditions of two kinds of arrays remain the same as above, and the configuration of the circular array is shown in Figure 10(a). Figure 10(b) shows the side nulls of the circular

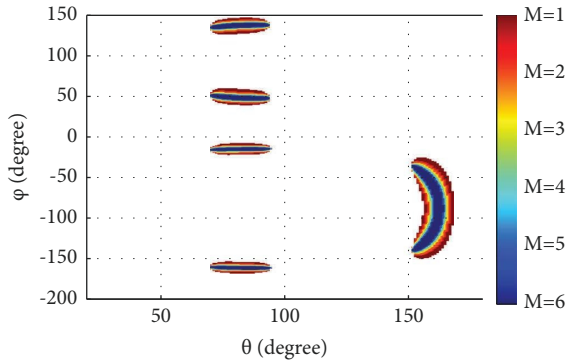

Figure 9: The side nulls of different number of auxiliary antennas.

Table 2: Proportion of side nulls with different number of auxiliary antennas.

Number of auxiliary antennas	Proportion of side nulls (%)
1	5
2	3.38
3	2.55
4	2.05
5	1.76
6	1.61

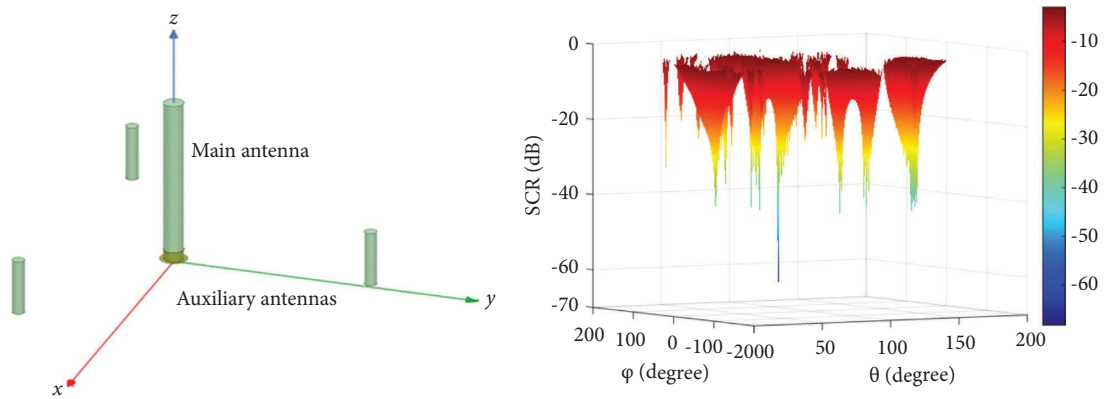

Figure 10: (a) The configuration of the circular array. (b) The side nulls of the circular array.

array when the array radius $r = \lambda$. It can be observed that, compared with the linear array in Figure 10(b), side nulls of the circular array increase significantly, accounting for about 11.2%. However, the side nulls become more dispersed in the pitch plane and decrease in the same azimuth plane. This means that the circular array has better direction finding in the azimuth plane.

4.4. Comparison and Analysis. It can be seen from above that the array manifold is important in side null reduction. The side null can be suppressed by adjusting the array. The method of array analysis is also used in some papers. The studies in [34] replaces the separate auxiliary antennas with a number of existing elements of the main antenna array in radar systems, and it maintains a distortionless response for the desired signal under high input SINR. It analyzes a number of various auxiliary configurations to validate the presented methods by comparing output SINR. The studies in [35] analyzes effect of auxiliary element position on performance of the side-lobe canceller by the numerical simulation of some auxiliary element combinations. It also compares the output SINR to reflect the performance of the array. It can be known that when there are various influencing

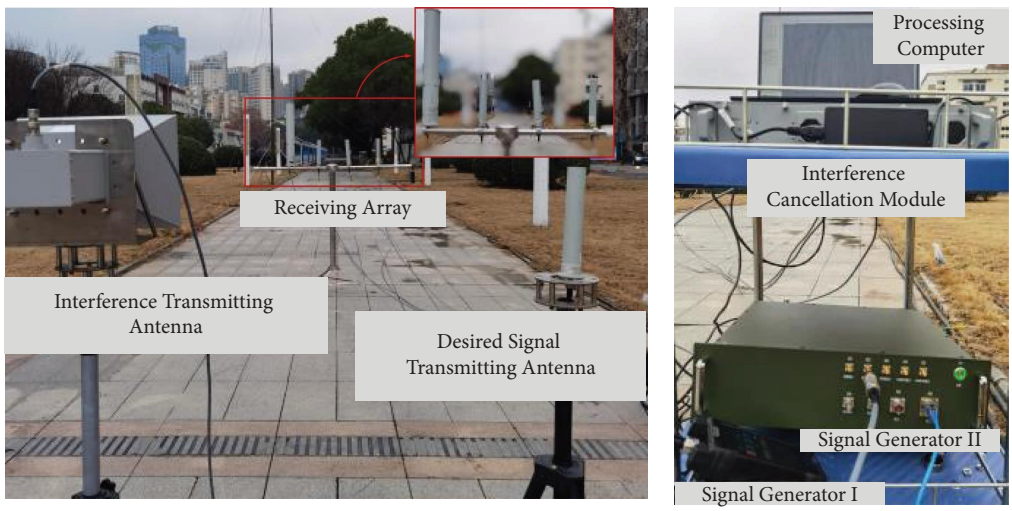

Figure 11: The scenario of experiment. (a) The transmitting and receiving antenna array. (b) Signal generators and processing module.

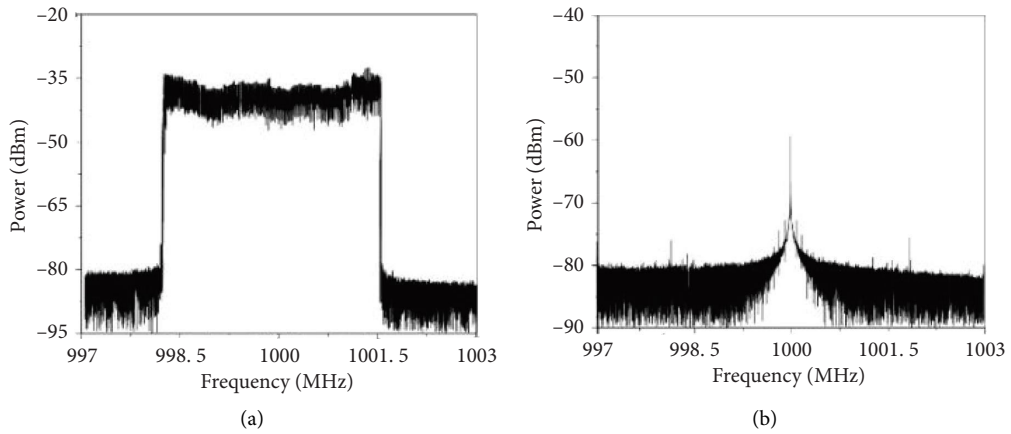

Figure 12: The frequency spectrum of interference signal and desired signal. (a) Interference signal. (b) Desired signal.

factors and the analytical solution cannot be obtained, the simulation of different arrays manifold is an effective analysis method.

5. Experimental Validation

Based on the above analysis and simulation, experiments are conducted to verify the side null. The experimental scenario is shown in Figure 11. Two signal generators are used to transmit signals. One transmits the single-tone signal as the desired signal, and the other transmits the white noise with bandwidth of 3 MHz as the interference signal. The input SNR and INR are 20 dB and 50 dB, respectively. The directional horn antenna is used as the interference-transmitting antenna, and the omnidirectional antenna is used as the desired signal-transmitting antenna. A main-auxiliary antenna array consisting of one main antenna and three uniformly linearly placed auxiliary antennas is used as the receiving array. Through adjusting the position of the transmitting antenna, different AoA of signals can be realized. The received signals are then transmitted to the interference cancellation module. The data are collected and processed in the computer. The output SNR can be obtained by calculation. The input SNR is decided by the input power of the desired signal and the background noise. According to equation (18), the SCR is obtained.

The element spacing is one wavelength, and the other experimental parameters are consistent with the simulation. Figure 12 shows the frequency spectrums of the desired signal and the interference signal. The AoA of the interference signal is $(90^\circ, 45^\circ)$. The AoA of the desired signal is chosen as $(90^\circ, 25^\circ)$ and $(90^\circ, -17^\circ)$, where $(90^\circ, -17^\circ)$ is in the side null. The frequency spectrums before and after interference cancellation at two AoA are shown in Figure 13. It is observed that the desired signal is submerged by the interference signal without interference cancellation. After interference cancellation, the interference signal is cancelled, and the desired signal is revealed. However, when the

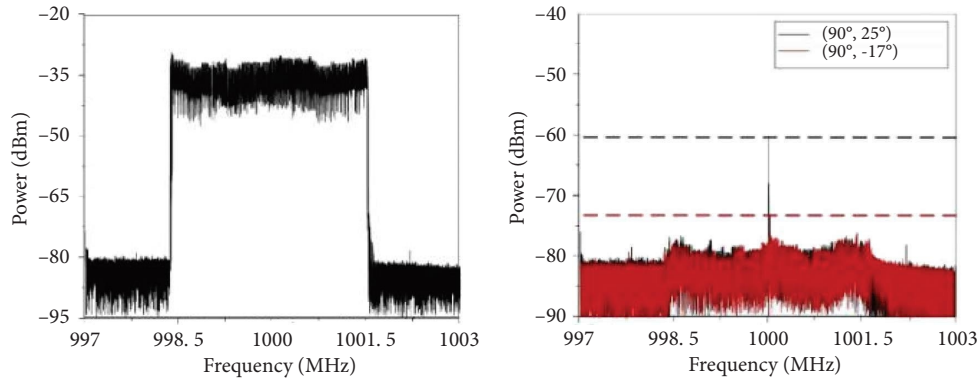

Figure 13: The frequency spectrum before and after interference cancellation. (a) Before interference cancellation. (b) After interference cancellation.

Table 3: The comparison of simulation and measurement in different arrival angles.

AoA of desired signal	Simulated SCR (dB)	Measured SCR (dB)
$(90^{\circ}, 137^{\circ})$	−23	−20
$(90^{\circ}, 85^{\circ})$	5	6
$(90^{\circ}, -75^{\circ})$	−2	−2
$(80^{\circ}, 45^{\circ})$	−16	−15
$(100^{\circ}, 45^{\circ})$	7	6

desired signal is from the side null of $(90^{\circ}, -17^{\circ})$, the desired signal is attenuated about 14 dB. When the desired signal is from $(90^{\circ}, 25^{\circ})$, the desired signal almost returns to the original level. Other five AoAs of the desired signal are measured in the experiments. The results are shown in Table 3. It is roughly consistent with the theoretical calculation and verifies that the desired signal is attenuated when it comes from the direction of the side null, which affects the effect of cancellation. The experimental results are in good agreement with the simulation. It proves the existence of side nulls and theoretical analysis.

6. Conclusion

In this paper, the side null of the main-auxiliary antenna array in noncooperative interference cancellation is analyzed. The null in the noninterference direction is described as the side null. When the AoA of the desired signal is in the side nulls, the effectiveness of interference cancellation is impaired even the interference signal is eliminated. This means that communication based on the desired signal cannot recover to the level before interference, and the effect of interference cancellation is negatively affected. To quantitatively characterize the side null, SCR is deduced through modeling interference cancellation of the main-auxiliary antenna array. The simulation and analysis in the two-dimensional plane and three-dimensional space intuitively describe the side null. Besides, the side null reduction is discussed through an adjusting array. It has been found that the side null suppression can be achieved by adjusting element spacing, increasing element number, and adjusting array configuration. Finally, the existence of side null and its effect on interference cancellation are verified by experiments. The analysis, simulation, and experiment agree well with each other. The concept and quantitative characterization of side null proposed in the paper and the discussion of side null reduction provide the basis for subsequent research of the array design in the noncooperative interference cancellation.

Data Availability

The data used to support the findings of this study are included within the article.

Conflicts of Interest

The authors declare that they have no conflicts of interest regarding the publication of this paper.

Acknowledgments

This work was supported in part by the National Key R&D Program of China (2021YFF1500100), the National Natural Science Foundation of China (Grant No. 62001496 and 52177012), The Young Elite Scientists Sponsorship Program by CAST, the National Fund for Distinguished Young Scholars (Grant No. 52025072), and the Foundation of National Key Laboratory of Science and Technology on Vessel Integrated Power System (Grant No. 6142217210501).

References

[1] B. Sun, Y. Zhou, J. Yuan, and J. Shi, "Interference cancellation based channel estimation for massive MIMO systems with time shifted pilots," *IEEE Transactions on Wireless Communications*, vol. 19, no. 10, pp. 6826–6843, 2020.

[2] X. Chen, T. Shu, K. B. Yu, J. He, and W. Yu, "Joint adaptive beamforming techniques for distributed array radars in multiple mainlobe and sidelobe jammings," *IEEE Antennas and Wireless Propagation Letters*, vol. 19, no. 2, pp. 248–252, 2020.

[3] W. Li, Z. Zhao, J. Tang, F. He, Y. Li, and H. Xiao, "Performance analysis and optimal design of the adaptive interference cancellation system," *IEEE Transactions on Electromagnetic Compatibility*, vol. 55, no. 6, pp. 1068–1075, 2013.

[4] D. J. Moelker, E. van der Pol, and Y. Bar-Ness, "Adaptive antenna arrays for interference cancellation in GPS and GLONASS receivers," in *Proceedings of the Position Location and Navigation Symposium-PLANS'96*, pp. 191–198, Atlanta, GA, USA, April 1996.

[5] M. A. Ahmed, A. Baz, and C. C. Tsimenidis, "Performance analysis of NOMA systems over Rayleigh fading channels with successive-interference cancellation," *IET Communications*, vol. 14, no. 6, pp. 1065–1072, 2020.

[6] F. Babich and M. Comisso, "Impact of segmentation and capture on slotted Aloha systems exploiting interference cancellation," *IEEE Transactions on Vehicular Technology*, vol. 68, no. 3, pp. 2878–2892, 2019.

[7] L. Shen, B. Henson, Y. Zakharov, and P. Mitchell, "Digital self-interference cancellation for full-duplex underwater acoustic systems," *IEEE Transactions on Circuits and Systems II: Express Briefs*, vol. 67, no. 1, pp. 192–196, 2020.

[8] J. R. Mohammed and K. H. Sayidmarie, "Null steering method by controlling two elements," *IET Microwaves, Antennas And Propagation*, vol. 8, no. 15, pp. 1348–1355, 2014.

[9] L. V. Tong, K. M. Kha, C. V. Nguyen, T. L. Nguyen, and G. B. V. Truong, "Null-steering beamformers for suppressing unknown direction interferences in sidelobes," *Journal of Communications*, vol. 17, no. 8, pp. 600–607, 2022.

[10] X. Wang, M. Amin, and X. Cao, "Analysis and design of optimum sparse array configurations for adaptive beamforming," *IEEE Transactions on Signal Processing*, vol. 66, no. 2, pp. 340–351, 2018.

[11] C. Wen, Y. Huang, J. Peng, G. Zheng, W. Liu, and J. K. Zhang, "Reconfigurable sparse array synthesis with phase-only control via consensus-ADMM-based sparse optimization," *IEEE Transactions on Vehicular Technology*, vol. 70, no. 7, pp. 6647–6661, 2021.

[12] Q. Wang, Y. Li, K. Luo, Q. Wang, F. He, and B. Li, "Auxiliary antenna array analysis and design for sidelobe interference cancellation of satellite communication system," *Progress in Electromagnetics Research M*, vol. 96, pp. 55–67, 2020.

[13] N. Rezazadeh and L. Shafai, "A compact antenna for GPS anti-jamming in airborne applications," *IEEE Access*, vol. 7, pp. 154253–154259, 2019.

[14] X. Yang, P. Yin, T. Zeng, and T. K. Sarkar, "Applying auxiliary array to suppress mainlobe interference for ground-based radar," *IEEE Antennas and Wireless Propagation Letters*, vol. 12, pp. 433–436, 2013.

[15] C. Hu, Z. Chen, X. Dong, and C. Cui, "Multistatic geosynchronous SAR resolution analysis and grating lobe suppression based on array spatial ambiguity function," *IEEE Transactions on Geoscience and Remote Sensing*, vol. 58, no. 9, pp. 6020–6038, 2020.

[16] H. Wang, D. G. Fang, and Y. L. Chow, "Grating lobe reduction in a phased array of limited scanning," *IEEE Transactions on Antennas and Propagation*, vol. 56, no. 6, pp. 1581–1586, 2008.

[17] W. Tian, Y. Li, J. Wang, C. Hu, and T. Zeng, "Design of MIMO array with low grating lobes in near-field imaging," in *Proceedings of the General Assembly and Scientific Symposium of the International Union of Radio Science (URSI GASS)*, pp. 1–4, Montreal, Canada, January 2017.

[18] R. Zhu, J. Zhou, Q. Fu, and G. Jiang, "Spatially variant apodization for grating and sidelobe suppression in near-range MIMO array imaging," *IEEE Transactions on Microwave Theory and Techniques*, vol. 68, no. 11, pp. 4662–4671, 2020.

[19] P. Saxena and A. Kothari, "Ant lion optimization algorithm to control side lobe level and null depths in linear antenna arrays," *AEU-International Journal of Electronics and Communications*, vol. 70, no. 9, pp. 1339–1349, 2016.

[20] K. Chen, X. Yun, Z. He, and C. Han, "Synthesis of sparse planar arrays using modified real genetic algorithm," *IEEE Transactions on Antennas and Propagation*, vol. 55, no. 4, pp. 1067–1073, 2007.

[21] W. Alshrafi, A. Al-Bassam, and D. Heberling, "Grating lobe mitigation in series-fed patch periodic leaky-wave antenna using parasitic monopoles," *IEEE Antennas and Wireless Propagation Letters*, vol. 19, no. 12, pp. 2472–2476, 2020.

[22] Z. Iqbal, T. Mitha, and M. Pour, "A self-nulling single-layer dual-mode microstrip patch antenna for grating lobe reduction," *IEEE Antennas and Wireless Propagation Letters*, vol. 19, no. 9, pp. 1506–1510, 2020.

[23] M. Y. Javed, N. Tervo, M. E. Leinonen, and A. Pärssinen, "Spatial interference reduction by subarray stacking in large two-dimensional antenna arrays," *IEEE Transactions on Antennas and Propagation*, vol. 69, no. 7, pp. 3863–3874, 2021.

[24] Y. Aslan, "Optimization of virtually aperiodic linear sparse arrays," *Microwave and Optical Technology Letters*, vol. 64, no. 2, pp. 318–324, 2022.

[25] Q. Lou and Z. N. Chen, "Sidelobe suppression of metalens antenna by amplitude and phase controllable metasurfaces," *IEEE Transactions on Antennas and Propagation*, vol. 69, no. 10, pp. 6977–6981, 2021.

[26] J. Ma, K. Li, J. Tian, X. Long, and S. Wu, "Fast sidelobe suppression based on two-dimensional joint iterative adaptive filtering," *IEEE Transactions on Aerospace and Electronic Systems*, vol. 57, no. 5, pp. 3463–3478, 2021.

[27] X. Yang, S. Li, T. Long, and T. K. Sarkar, "Adaptive null broadening method in wideband beamforming for rapidly moving interference suppression," *Electronics Letters*, vol. 54, pp. 1003–1005, 2018.

[28] L. T. Van and T. V. B. Giang, "Interference suppression of ULA antennas by phase-only control using bat algorithm," *IEEE Antennas and Wireless Propagation Letters*, vol. 16, pp. 3038–3042, 2017.

[29] X. Wang, E. Aboutanios, M. Trinkle, and M. G. Amin, "Reconfigurable adaptive array beamforming by antenna selection," *IEEE Transactions on Signal Processing*, vol. 62, no. 9, pp. 2385–2396, 2014.

[30] K. L. Collier and L. L. Joiner, "A collaborative technique for spatial interference reduction in multi-node antenna arrays with antenna diversity," in *Proceedings of the 2018 IEEE/ION Position, Location and Navigation Symposium (PLANS)*, pp. 92–101, Monterey, CA, USA, April 2018.

[31] Y. X. Zhang, Y. C. Jiao, and L. Zhang, "Antenna array directivity maximization with sidelobe level constraints using convex optimization," *IEEE Transactions on Antennas and Propagation*, vol. 69, no. 4, pp. 2041–2052, 2021.

[32] A. Pal, A. Mehta, A. Skippins, P. Spicer, and D. Mirshekar-Syahkal, "Novel interference suppression null steering antenna system for high precision positioning," *IEEE Access*, vol. 8, pp. 77779–77787, 2020.

[33] Y. Lu, J. Ma, L. Shi, and Y. Quan, "Multiple interferences suppression with space-polarization null-decoupling for polarimetrie array," *Journal of Systems Engineering and Electronics*, vol. 32, no. 1, pp. 44–52, 2021.

[34] J. R. Mohammed and K. H. Sayidmarie, "Performance evaluation of the adaptive sidelobe canceller system with various auxiliary configurations," *AEU-International Journal of Electronics and Communications*, vol. 80, pp. 179–185, 2017.

[35] Z. Zhang, Z. Xu, and Y. Liu, "Effect of auxiliary element position on performance of sidelobe canceller," *Modern Radar*, vol. 44, no. 9, pp. 7–12, 2022.